Organometallic ionic liquids from alkyloctamethylferrocenium cations: Thermal properties, crystal structures, and magnetic properties

Funasako, Yusuke ; Inagaki, Takashi ; Mochida, Tomoyuki ; Sakurai, Takahiro ; Ohta, Hitoshi ; Furukawa, Ko ; Nakamura, Toshikazu

(Citation)
Dalton transactions,42(23):8317-8327

(Issue Date)
2013-04-04

(Resource Type)
journal article

(Version)
Accepted Manuscript

Organometallic Ionic Liquids from Alkyloctamethylferrocenium Cations: Thermal Properties, Crystal Structures, and Magnetic Properties†

Yusuke Funasako,[a] Takashi Inagaki,[a] Tomoyuki Mochida,*[a] Toshihiro Sakurai,[b] Hitoshi Ohta,[c] Ko Furukawa[d,‡] and Toshikazu Nakamura[d]

Abstract: Alkyloctamethylferrocenium salts with the Tf_2N anion ($[Fe(C_5Me_4C_nH_{2n+1})(C_5Me_4H)][Tf_2N]$; Tf_2N = bis(trifluoromethanesulfonyl)amide) were prepared, and their ionic liquid properties, thermal properties, crystal structures, and magnetic properties were investigated. The melting points of the Tf_2N salts were near room temperature, and decreased with increasing alkyl chain length up to n = 8 and then increased. The salts with PF_6 and NO_3 anions were also prepared. The melting points of the PF_6 salts were higher than 100 °C. Most of these salts exhibited phase transitions in the solid state. The sum of the entropies of the melting and solid phase transitions was nearly independent of the alkyl chain length for salts with short alkyl chains, whereas those for salts with longer alkyl chains ($n \geq 10$ for Tf_2N salts, $n \geq 6$ for PF_6 salts) increased with increasing alkyl chain length. Crystal structure determinations revealed that the short chain salts form simple alternately packed structures of cations and anions in the solid state, and that the long chain salts form lamellar structures, in which the alkyl chains are aligned parallel between the layers. The effects of magnetic fields on crystallization of the paramagnetic ionic liquids were investigated, and revealed that the Tf_2N salts with n = 4 exhibited magnetic orientation when solidified under magnetic fields. The magnetic orientation was shown to be a bulk phenomenon, and the importance of the magnetic anisotropy of the crystal structure was suggested in comparison with the response of other Tf_2N salts.

1. Introduction

Ionic liquids are salts with melting points below 100 °C, and they are intriguing from the viewpoint of fundamental physical chemistry and electrochemistry.[1] Most ionic liquids are formed from organic onium cations such as imidazolium, ammonium, and phosphonium cations, and their modifications have led to various functionalities.[2] As the counter anion, fluorinated anions such as bis(trifluoromethanesulfonyl)amide (Tf_2N) are frequently used, and magnetic anions such as MX_n (M = metal, X = anionic ligands),[3] organic radicals,[4] and metal complexes[5] are used to add magnetic functions to the liquids.

Recently, several interesting examples of onium-free ionic liquids composed of cationic metal complexes have been reported.[6] We have recently developed ionic liquids containing metallocenium cations[7] and cationic chelate complexes,[8] which exhibit interesting properties such as magnetic orientation,[7b,7d] color changes,[8a] gas absorption,[7e,8a] and chemical reactivities.[7e] Ferrocenium cations are interesting from the viewpoint of magnetism,[9] and they are suitable as components of ionic liquids because of their bulkiness and charge delocalization. However, ferrocenium ionic liquids are highly sensitive to air.[7a,7d] In this study, alkyloctamethylferrocenium cations were used to achieve air-stable ferrocenium ionic liquids. There are a few examples of liquid-like peralkylated ferrocenium salts, such as alkali metal podates with ether substituents[10] and liquid crystal salts with mesogenic substituents.[11]

In this paper, we report the preparation and physical properties of alkyloctamethylferrocenium salts with the Tf_2N anion ($[Fe(C_5Me_4C_nH_{2n+1})(C_5Me_4H)][Tf_2N]$, Scheme 1), which are air-stable paramagnetic ionic liquids. 1-Pentenyloctamethylferrocene was also used as the cation, and several nitrate (NO_3) and hexafluorophosphate (PF_6) salts were prepared for comparison. Discussion of the crystal structure is useful in elucidating the nature of ionic liquids.[12] Although structural data were not available for the ferrocenium ionic liquids, structural determination of the present salts was possible.

The thermal properties of [**C6Fc**][Tf_2N][7c] and the effects of magnetic fields on the crystallization of [**C4Fc**][Tf_2N][7b] have been reported previously. A detailed investigation of magnetic phenomena in the latter salt is described here, and compared with those of other Tf_2N salts.

2. Results and Discussion

Preparation and properties

The alkyloctamethylferrocenium salts were prepared according to Scheme 2. Octamethylformylferrocene was reacted with Grignard reagents, and the resultant alcohols were reduced to give alkyloctamethylferrocenes as yellow-orange oils, which were further reacted with AgX (X = Tf_2N, PF_6, and NO_3) to give the desired salts. The Tf_2N salts ([**C3Fc**][Tf_2N]–[**C17Fc**][Tf_2N]) were obtained as dark-green oils or solids, which were stable under air. The 1-pentenyl derivative [**C5'Fc**][Tf_2N] was prepared similarly. The melting points (T_m) of the Tf_2N salts were in the range 15–70 °C. The PF_6 salts ([**C4Fc**][PF_6], [**C6Fc**][PF_6], [**C10Fc**][PF_6]) and NO_3 salts ([**C6Fc**][NO_3] and [**C10Fc**][NO_3]) were obtained as dark-green solids. The melting points of these salts were above 100 °C except for [**C10Fc**][NO_3], which melted at about 80 °C.

Melting points of Tf_2N salts and their precursors

The melting points, melting entropies, and glass transition temperatures of the Tf_2N salts are listed in Table 1. The melting points are plotted in Fig. 1 as a function of the alkyl chain length. Compared with [$Fe(C_5Me_4H)_2$][Tf_2N] (T_m = 213 °C),[13] introduction of alkyl chains significantly decreased the melting points. The melting points decreased with increasing chain length up to n = 8 and then increased, where n is the number of carbon atoms in the chain. This tendency is similar to that observed in ionic liquids of alkylimidazolium salts.[14] The melting points of the present salts are higher by 10–30 °C than those of

[Rmim][Tf_2N] (Rmim = 1-alkyl-3-methylimidazolium)[14b] and [Fe(C_5H_4R)(C_5H_5)][Tf_2N][7a,7d] with the same alkyl chain lengths, which is consistent with the larger molecular weights and volumes of the cations. The melting point of the alkenyl derivative [**C5'Fc**][Tf_2N] (T_m = 56.9 °C) was higher than that of the alkyl derivative [**C5Fc**][Tf_2N] (T_m = 30.0 °C and 20.2 °C, vide infra) as a result of the decreased flexibility of the substituent.

The thermal properties of alkyloctamethylferrocenes, which are the precursors of the salts, were also examined (Table 2). They melted at around 20 °C, and exhibited glass transitions at around –85 °C when cooled from the liquid state. Crystallization was observed in the heating process from the glassy state, except for the pentyl and 1-pentenyl derivatives. It is interesting that the melting points of alkyloctamethylferrocenes (open circles) and their Tf_2N salts (filled circles) are comparable (Fig. 1).

The ratios of the melting points and glass transition temperatures (T_g/T_m) for the alkyloctamethylferrocenes were 0.61–0.65. In the Tf_2N salts, the glass transition was only observed in the pentenyl derivative [**C5'Fc**][Tf_2N] (T_g = –67 °C) when the liquid was cooled at a rate faster than 10 °C min^{-1}. The T_g/T_m ratio for this salt was 0.62. These ratios are consistent with the empirical relationship ($T_g/T_m \approx 2/3$) known for general molecular compounds[15] and also for alkylimidazolium ionic liquids.[16]

Table 1 Melting points (T_m), melting entropies (ΔS_m), phase transition temperatures (T_{c1}, T_{c2}), phase transition entropies (ΔS_{c1}, ΔS_{c2}), and the sums of the phase transition entropies (ΔS_{total}) of the Tf_2N, PF_6, and NO_3 salts.

	T_m / °C	ΔS_m / J K^{-1} mol^{-1}	T_{c1} / °C	ΔS_{c1} / J K^{-1} mol^{-1}	T_{c2} / °C	ΔS_{c2} / J K^{-1} mol^{-1}	ΔS_{total}[a] / J K^{-1} mol^{-1}
[**C3Fc**][Tf_2N]	67.4	16.6	45.4	90.5			107.1
[**C4Fc**][Tf_2N]	34.4	86.3					86.3
[**C5Fc**][Tf_2N]	30.0	98.5					98.5
	20.2[b]	20.4	0.5[b]	44.0[b]			–
[**C5'Fc**][Tf_2N]	56.9	80.7					80.7
[**C6Fc**][Tf_2N]	27.7	27.4	21.4	55.2			84.6
			–1.6[b]	39.7[b]			
[**C8Fc**][Tf_2N]	16.9	12.5	1.7	19.9	11.5	2.5	34.9
[**C10Fc**][Tf_2N]	17.5	12.5	11.0	14.7			27.2
[**C12Fc**][Tf_2N]	26.2	18.0	8.7	36.5			54.5
[**C17Fc**][Tf_2N]	56.8	97.3					93.6
[**C4Fc**][PF_6]	166.8	26.1	–53.8	4.4	108.1	28.6	59.1
[**C6Fc**][PF_6]	142.1	26.7	109.9	1.1	132.2	7.3	35.1
[**C10Fc**][PF_6]	201.4	39.8	–44.5	20.5	49.2	7.0	64.3
			54.2[b]	32.9[b]			
[**C6Fc**][NO_3]	109.4	26.6					26.6

[a] $\Delta S_{total} = \Delta S_m + \Delta S_{c1} + \Delta S_{c2}$. [b] Phase transitions in metastable polymorphs.

Table 2 Melting points (T_m), melting entropies (ΔS_m), and glass transition temperatures (T_g) of alkyloctamethylferrocenes.

	T_m / °C	ΔS_m / J K^{-1} mol^{-1}	T_g / °C
C3Fc	17.5	68.9	–97
C4Fc	27.6	80.6	–88
C5Fc	–	–	–86
C5'Fc	–	–	–84
C6Fc	22.1	84.7	–83
C8Fc	23.8	34.7	–84

Phase transitions in the Tf_2N salts

The phase sequences of the Tf_2N salts are shown in Fig. 2. [**C4Fc**][Tf_2N], [**C5'Fc**][Tf_2N], and [**C17Fc**][Tf_2N] exhibited only melting and crystallization (Fig. 2a), and no phase transitions were observed in the solid state. [**C3Fc**][Tf_2N], [**C10Fc**][Tf_2N], and [**C12Fc**][Tf_2N] exhibited one phase transition and [**C8Fc**][Tf_2N] exhibited two phase transitions in the solid state (Fig. 2b). The large values of ΔS indicate that extensive molecular motions occur above the phase transition temperatures, not merely rotational and/or conformational disorder of anions.

The high-temperature phases in these salts are orientationally disordered phases with small melting entropies (ΔS < 20 J K^{-1} mol^{-1}).[17] Among them, [**C10Fc**][Tf_2N] showed a glass transition in the crystal

phase (phase II) at –40 °C, where the motions of the alkyl chains are probably frozen to form a glassy crystal. [**C5Fc**][Tf_2N] and [**C6Fc**][Tf_2N] exhibited three crystal phases, including metastable phases (Fig. 2c). The differential scanning calorimetry (DSC) traces for [**C5Fc**][Tf_2N] are shown in Fig. S1 in the ESI†. The Gibbs free energy diagram for this salt derived from the data is shown in Fig. 3. The melting points of the stable phase (phase III) and the metastable phase (phase I) were 30.0 °C and 20.2 °C, respectively, and their melting entropies (ΔS_m) were 98.5 J K^{-1} mol^{-1} and 20.4 J K^{-1} mol^{-1}, respectively. The latter small entropy indicates that phase I is a highly disordered phase. [**C6Fc**][Tf_2N] showed a similar but slightly different behavior, which we reported previously.[7c]

The sums of the entropies of the melting and solid phase transitions for the Tf_2N salts (ΔS_{total}) are shown in Fig. 4. The values for the salts with n = 3, 4, 5, and 6 were comparable (80–110 J K^{-1} mol^{-1}), whereas the salt with n = 8 exhibited a much smaller value, and the salts with $n \geq 10$ displayed an increase with elongation of the alkyl chain. For molecules consisting of a rigid core and alkyl chains, such as mesogens and alkylimidazolium ionic liquids, conformational changes of the alkyl chains provide an entropy change of about 10 J K^{-1} mol^{-1} per methylene unit.[18] The Tf_2N salts with $n \geq 10$ followed this tendency well, which indicates that the motion of the alkyl groups dominates the phase change entropies in these salts. The absence of such a tendency in the salts with $n \leq 6$ is partly because the entropy contributions from the alkyl moieties are small in the short chain salts, and, moreover, is probably the result of different packing structures (vide infra). The total phase transition entropy in [**C5'Fc**][Tf_2N] (80.7 J K^{-1} mol^{-1}) was smaller by about 20 J K^{-1} mol^{-1} than that in [**C5Fc**][Tf_2N] (98.5 J K^{-1} mol^{-1}), which is consistent with the loss of rotational freedom of two methylene groups.

It is interesting to note that the total phase transition entropies of alkyloctamethylferrocenes and the Tf_2N salts are comparable (Fig. 4 and Table 2), as well as the melting points, as noted above. A linear correlation between the melting points of the salts and the precursors has also been observed in

alkylferrocenium Tf_2N salts.[7d] These results demonstrate that the thermodynamic properties of the Tf_2N salts reflect those of their precursors.

Thermal properties of PF_6 and NO_3 salts

The melting points of [**C4Fc**][PF_6], [**C6Fc**][PF_6], and [**C10Fc**][PF_6] were 166.8 °C, 142.1 °C, and 201.4 °C respectively, and they first decreased and then increased with increasing chain length. The melting points of the PF_6 salts were higher by 100–150 °C than those of the corresponding Tf_2N salts. The PF_6 salts exhibited phase transitions in the solid state, showing three stable crystalline phases (phase I–III). Their phase transition data are shown in Table 1. Among them, [**C10Fc**][PF_6], obtained by recrystallization, was a metastable glassy crystal, which was transformed to the stable phase (phase I) by heating (Fig. S2 in the ESI†). The sums of the phase transition entropies for the salts with n = 4, 6, and 10 were 59.1 J K^{-1} mol^{-}, 35.1 J K^{-1} mol^{-}, and 64.3 J K^{-1} mol^{-1}, respectively. The dependence on n is similar to that observed in the Tf_2N salts shown above. The increase in the value for the last salt is accounted for by the increased alkyl chain length, and the different tendency for the salt with n = 4 is ascribed to different packing structures, as shown below.

The melting point of [**C6Fc**][NO_3] was 109.4 °C (ΔS = 26.6 J K^{-1} mol^{-1}), which is much higher than that of the corresponding Tf_2N salt ([**C6Fc**][Tf_2N]: T_m = 27.7 °C). Crystallization from the melt occurred at 23.5 °C when cooled at 2 °C min^{-1}, but a glass transition (T_g = –35 °C) was observed when the cooling rate was faster than 10 °C min^{-1}. [**C10Fc**][NO_3] melted at around 80–82 °C, but it is not precise melting points because of small amounts of remaining solvate molecules.

Viscosities

The viscosities of [**C6Fc**][Tf_2N] and [**C10Fc**][Tf_2N] at 25 °C were 752 mPa s and 746 mPa s, respectively, and they were comparable. Both were Newtonian liquids, and they were much more viscous than the imidazolium ionic liquids (e.g., [bmim][Tf_2N]: 49 mPa s, bmim = 1-butyl-3-methylimidazolium)[19] and ferrocenium ionic liquids (e.g., [Fe($C_5H_4{}^nBu$)(C_5H_5)][Tf_2N]: 112.3 mPa s).[7a,7d] The temperature dependences of the viscosities were fitted using the Arrhenius plot, from which activation energies (E_a) of 43.1 kJ mol^{-1} and 44.9 kJ mol^{-1}, respectively, were derived. These values are comparable to those of [bmim][Tf_2N] (31.3 kJ mol^{-1})[19] and [Fe($C_5H_4{}^nBu$)(C_5H_5)][Tf_2N] (38.8 kJ mol^{-1}).[7a,7d] The Vogel–Tammann–Fulcher (VTF) equation ($\eta = \eta_0 \exp[DT_0/(T-T_0)]$)[20] was also used to fit the data, where T_0 is the ideal glass transition temperature and D is a parameter that shows deviation from Arrhenius behavior. The values T_0 and D obtained for [**C6Fc**][Tf_2N] were –57.2 °C and 1.76, and those for [**C10Fc**][Tf_2N] were –53.6 °C and 1.63, respectively. The small D values, which are even smaller than that of [bmim][Tf_2N] (D = 4.65),[21] suggest that they are strongly fragile liquids.[22]

Crystal structures

The crystal structures of [**C3Fc**][Tf_2N], [**C4Fc**][PF_6], [**C6Fc**][X], and [**C10Fc**][X] (X = PF_6, NO_3) were determined at –100 °C. Their packing diagrams are shown in Fig. 5. The structure of [**C4Fc**][Tf_2N] was reported previously.[7b] [**C3Fc**][Tf_2N] belongs to space group $C2/c$, [**C4Fc**][PF_6] and [**C10Fc**][NO_3] belong to $P\bar{1}$, and the others belong to $P2_1/c$. In the alkyl chains of the salts, the C–C bond adjacent to the Cp ring exhibited the *gauche* conformation, whereas the other bonds exhibited the *trans* conformation. [**C4Fc**][PF_6] exhibited disorder in the alkyl chains. The intramolecular Fe–C(Cp) bond lengths, of which Fe–C_H was the shortest, were comparable to those of substituted octamethylferrocenium cations.[23] In all the salts, the C_5 axes of the ferrocenium moieties were aligned in nearly the same direction in the crystal. Weak hydrogen bonds were formed in the NO_3 and PF_6 salts

between the ring hydrogen of the cation and the oxygen or fluorine atom in the anion (Fig. S3 in the ESI†). The CH...X (X = O or F) distances were shorter than the van der Waals distances by 0.15–0.36 Å. The Tf_2N salts exhibited no such contacts.

The packing arrangements of the salts depended on the alkyl chain length in the cation. In the salts with short alkyl chains ([**C3Fc**][Tf_2N] and [**C4Fc**][PF_6]), the anions and cations are packed alternately in the unit cell (Figs 5a–b). [**C4Fc**][Tf_2N] also exhibited a similar structure.[7b] In contrast, lamellar structures are formed in the salts with longer alkyl chains ([**C6Fc**][X] and [**C10Fc**][X]; X = PF_6, NO_3) (Figs. 5c–f). In these crystals, the anions and cations are arranged alternately to form layers, which are stacked with their alkyl chains extending outside the layers. The alkyl chains are in contact with each other between the layers and there are no direct π–π interactions between the cations. The interlayer distances in [**C10Fc**][X] are longer than those in [**C6Fc**][X] as a result of the longer alkyl chains. In the salts, except for [**C10Fc**][NO_3], the C_5 axes of the ferrocenium moieties are aligned parallel to the stacking direction of the layers. The difference between the packing patterns of the long chain and short chain salts, giving different lattice entropies, accounts for the observed different tendencies of the phase change entropies. A similar phenomenon has been observed in cobaltocenium salts.[24] Although the crystal structures of the Tf_2N salts with long alkyl chains were not determined, it is likely that the Tf_2N salts with $n \geq 8$ form lamellar structures, considering the tendency of the phase transition entropies in Fig. 4.

Magnetic properties of [C4Fc][Tf_2N]

The Tf_2N salts are paramagnetic ionic liquids containing magnetically anisotropic paramagnetic cations. We investigated the effects of magnetic fields on their crystallization. A remarkable effect was found in [**C4Fc**][Tf_2N], which we reported previously in a communication[7b] and briefly describe here. As shown

in Fig. 6 (open circles), when the liquid was cooled under a magnetic field (0.5–2 T), the magnetic susceptibility suddenly increased upon solidification at 26 °C, and, when heated, the value decreased again to the liquid value at 36 °C upon melting. The magnetic field affected the susceptibility increase, which increased with increasing field strength, but not the phase transition temperature.[7b] A similar magnetic response was also found in a ferrocenium ionic liquid $[Fe(C_5H_4Et)_2][Tf_2N]$,[7d] albeit with less reproducibility and controllability. We ascribe this phenomenon to magnetic orientation, and detailed investigations of the phenomenon are described below. To confirm the magnetic orientation of the field-cooled sample, we first measured the anisotropy of the magnetic susceptibility. A liquid sample of [**C4Fc**][Tf_2N] was crystallized under a magnetic field of 0.59 T, and the magnetic susceptibility (χT value) of this sample measured under a perpendicular field was 0.63 emu K mol^{-1} (Fig. 6, filled circles), which was smaller than that in the liquid state, whereas the value measured under the parallel field increased. This result directly demonstrates that the orientation of the crystal is controlled by the direction of the magnetic field.

The magnetic susceptibility of [**C4Fc**][Tf_2N] solidified under a field of 0.8 T was 1.36 emu K mol^{-1} when measured under a parallel field,[7b] whereas the value for a fully oriented sample is calculated to be 1.73 emu K mol^{-1}, using $\chi T = [g^2 S(S+1)]/8$, where $g_{//} = 4.3$ and $S = 1/2$. Assuming that there are only two components in the sample, fully oriented fraction and non-oriented isotropic fraction, the ratio of the former fraction was calculated to be 0.61 from the susceptibility values.

The magnetic orientation was further investigated using ESR spectroscopy. In the ESR spectra of an oriented polycrystalline sample crystallized under 0.8 T, a sharp, symmetrical peak was observed below –233 °C for a parallel orientation of the magnetic fields for crystallization and ESR measurements (Fig. S4a in the ESI†). In contrast, asymmetric peaks typical of a non-oriented material were observed for the sample crystallized without magnetic fields (Fig. S4b in the ESI†). Furthermore, a clear angular

dependence was observed in the ESR spectra of the oriented sample recorded at –269.4 °C, as shown in Fig. 7. An upfield shift and broadening of the peak were observed with increasing angle (θ) between the magnetic fields for the measurement and crystallization. The $g_{//}$ component along the C_5 axis of the cation is observed for $\theta = 0°$, and the $g_{\perp}$ component appears with sample rotation. The small residual peak of the $g_{//}$ component observed even for $\theta = 90°$ is a non-oriented fraction. Thus, the spectrum for each rotation angle contains the angular-dependent component of the oriented fraction and angular-independent component of the isotropic fraction (Fig. S5 in the ESI†). The *g*-values obtained by fitting the angular dependence (Fig. 7, inset) were $g_{//} = 4.3$, $g_{\perp} = 1.7$, and $g_{av} = 2.84$, which are comparable to the typical values for ferrocenium salts such as $[Fe(C_5Me_5)_2][PF_6]$ ($g_{//} = 4.43$, $g_{\perp} = 1.35$, $g_{av.} = 2.78$) and $[Fe(C_5Me_4H)_2][BF_4]$ ($g_{//} = 4.11$, $g_{\perp} = 1.42$, $g_{av.} = 2.64$).[25] The *g*-value calculated form the χT value in the liquid state (0.78 emu K mol^{-1}) was 2.87, which is in good agreement with the analysis. The linewidths and intensities of the $g_{//}$ and $g_{\perp}$ peaks were obtained by fitting the spectra, and then the peak areas of the angle-dependent and independent components were calculated from the simulated spectra for $\theta = 0°$ and $\theta = 90°$, respectively. The ratio of the former component, which corresponds to the ratio of the oriented fraction, was 0.6. The value is again in good agreement with that estimated from the magnetic susceptibility data (0.61) as shown above.

Mechanism of magnetic orientation in [C4Fc][Tf$_2$N]

To investigate the mechanism of the magnetic-field effect, the direction of the magnetic orientation was examined using powder X-ray diffraction (XRD) measurements. A liquid sample of [**C4Fc**][Tf_2N] was placed on a glass plate and crystallized under the magnetic field (0.36 T) of a neodymium magnet placed below the plate. The XRD patterns showed a significant increase in the intensity of the peaks at $2\theta =$

13°, 14.5°, and 23° for the out-of-plane measurement compared with that of an unoriented sample (Fig. S6 in the ESI†), but the crystal structure was unchanged by the magnetic field. The peak at $2\theta = 14.5°$ was indexed as (200), which shows that the *a*-axis, along which the C_5 axis of the cation is oriented, is oriented along the magnetic field, in agreement with the magnetic anisotropy of the crystal.[7b] In repeated experiments on the oriented samples, differences were observed in the relative peak intensities; this results from an in-plane distribution of the growth direction. The crystal growth pattern on the surface accompanying radial distribution was visually observable under a polarized optical microscope.[7b]

The effect of sample shape on the magnetic response was also investigated. For liquid samples in fine tubes (inner diameter 0.2 mm) or in the form of thin layers (thickness 0.5 μm), no magnetic orientations were observed, even under 7 T. Magnetic orientation was also inhibited by adding quartz wool to the liquid.[7b] In these circumstances, the orientation of the crystal growth may be affected largely by the surface rather than by the external fields. These results indicate that magnetic orientation is a bulk property, and that the phenomenon is not attributable to the orientation of independent molecules, but is more likely a result of orientation of the crystal nucleus or crystal growth direction during crystallization. This seems to be consistent with the less controllable response in a ferrocenium ionic liquid, $[Fe(C_5H_4Et)_2][Tf_2N]$, with a much lower viscosity than the present salt,[7d] because the slower crystallization of high-viscosity liquids may lead to better magnetic-field orientation. There might be a critical size of crystal nucleus for magnetic orientation, and further investigations may be needed to explore its microscopic mechanism. The above results unfortunately suggest that the fabrication of thin-layer magnetic memory devices based on this mechanism is unfeasible.

Magnetic properties of [C5'Fc][Tf_2N] and [C12Fc][Tf_2N]

In contrast to [**C4Fc**][Tf_2N], no significant magnetic orientation was observed in [**C5'Fc**][Tf_2N] and [**C12Fc**][Tf_2N]. The magnetic susceptibility of [**C5'Fc**][Tf_2N] increased by only 0.05 emu K mol^{-1} (0.73 emu K mol^{-1}) upon crystallization at –16 °C under 2 T (Fig. S7 in the ESI†), and, with heating, the value returned to the liquid value at 57 °C. Although the crystal structure is unknown, the negligible magnetic change can probably be ascribed to the small magnetic anisotropy of the crystal, if any.

When [**C12Fc**][Tf_2N] was cooled from the liquid phase, it crystallized into a disordered phase at 25 °C, which further exhibited a phase transition in the solid state at around 7 °C. The temperature dependences of the magnetic susceptibility upon cooling under 0.5 T, 1 T, and 7 T are shown in Fig. 8. Repeated experiments showed that this salt exhibited small, random changes of the χT values at the phase transitions, but the direction of the change was random, indicating that no orientation is caused by the magnetic fields. The χT value in the liquid state was 0.76 emu K mol^{-1}, which increased or decreased by less than 0.05 emu K mol^{-1} upon crystallization, and the value further increased or decreased by about 0.1 emu K mol^{-1} at the solid phase transition temperature. The absence of magnetic orientation in this salt is probably correlated with the rotational motion of the ferrocenium moiety, probably present in the disordered phase, which reduces the magnetic anisotropy of the crystal. The larger change in susceptibility observed at the solid phase transition is ascribed to the increased magnetic anisotropy of the crystal caused by ordering of the cation. In the solid phase transition, the orientations of the cations are fixed according to the crystal lattice, hence they are not affected by magnetic fields.

These results show that not all ferrocenium ionic liquids show a magnetic orientation effect, despite the magnetic anisotropy of the molecule, and that the phenomenon is instead related to the crystal properties. The orientation mechanism is therefore significantly different from the well-known magnetic orientation of diamagnetic liquid crystal molecules. The magnetic-field alignments of materials upon

solidification have attracted much interest,[26] and magnetic susceptibility changes coupled with a liquid–solid transformations have also been observed in several molecular materials such as paramagnetic ionic liquids[4,27] and a solid composed of radical dimers.[28] The magnetic orientation of metallomesogens coupled with a phase transition to a liquid crystalline phase is an interesting phenomenon.[29] In [**C4Fc**][Tf_2N], the magnetic orientation occurs near room temperature with hysteresis and with a large susceptibility change, the degree of which can be controlled by the strength of the applied field. These are unique magnetic switching properties not seen in other materials.

3. Conclusion

A series of alkyloctamethylferrocenium salts with Tf_2N, PF_6, and NO_3 anions ([$Fe(C_5Me_4C_nH_{2n+1})(C_5Me_4H)$][X]) were prepared. Investigation of their thermal properties, phase transition behaviors, and crystal structures revealed the following. The Tf_2N salts are ionic liquids that are stable under air. The alkyl chain length dependences of the melting points are similar to those observed for ionic liquids of alkylimidazolium salts. Most of the salts exhibit phase transitions in the solid state. In the salts with short alkyl chains, the sum of the phase change entropies is nearly constant, whereas the salts with longer alkyl chains display an entropy increase with elongation of the alkyl chain. Crystal structure determinations revealed that the short chain salts exhibit alternate stacking of cations and anions, whereas the long chain salts form lamellar structures, where the alkyl chains are aligned between the layers. The effect of magnetic fields on crystallization of the Tf_2N salts was investigated in detail. The magnetic orientation phenomenon in the salt with $n = 4$ upon crystallization originates from the magnetic anisotropy of the crystal structure, which is a bulk property. Further investigation of these functional liquids should lead to novel molecular electronic applications.

Experimental

General

Octamethylformylferrocene[30] and silver bis(trifluoromethylsulfonyl)amide ($AgTf_2N$)[31] were synthesized according to literature methods. The preparations of butyloctamethylferrocene and its Tf_2N salt ([**C4Fc**][Tf_2N]) were reported previously.[7b] Other reagents and solvents were commercially available. ^1H NMR spectra were recorded using a JEOL JNM-ECL-400 spectrometer. Elemental analyses were performed using a Yanaco CHN MT5 analyzer. DSC measurements were performed using a TA Instrument Q100 calorimeter in the temperature range –180 to 210 °C at a rate of 10 °C min^{-1}. The viscosities of the liquids were measured under N_2 atmosphere using a Toki Sangyo TV-22 viscometer with a 3° × R7.7 cone rotor, in the temperature range 14–36 °C. XRD data for the powder samples were recorded on a Rigaku SmartLab diffractometer using Cu Kα radiation (λ = 1.54056 Å). ESR spectra were recorded on an X-band JEOL TE-260 spectrometer in the temperature range –269.4 to –233 °C. For the ESR measurements, a powder sample of [**C4Fc**][Tf_2N] was loaded into a quartz tube, which was sealed under nitrogen, and the sample was heated to melt it. The field-oriented samples were prepared by cooling the sample to crystallize under the magnetic field of the ESR magnet (0.8 T). The non-oriented samples were obtained by the same procedure, without applying magnetic fields.

Preparation of Propyloctamethylferrocene

(a) 1-Hydroxypropyloctamethylferrocene. All the manipulations were carried out under a nitrogen atmosphere. Ethyl bromide (1.0 mL, 12.8 mmol) was added dropwise to a stirred mixture of magnesium turnings (0.330 g, 13.6 mmol) and ether (15 mL), and the solution was stirred until most of the magnesium dissolved. The Grignard reagent thus prepared was added slowly to a solution of octamethylformylferrocene (0.30 g, 1.0 mmol) in dry THF (20 mL) cooled at –78 °C, and the solution

was stirred for 30 min. The reaction mixture was quenched at –78 °C with saturated NH_4Cl solution (20 mL) and extracted with ether. The organic layer was dried over magnesium sulfate and concentrated under reduced pressure. The crude product was purified by column chromatography (silica, CH_2Cl_2). The product was obtained as a yellow solid (0.324 g, 99.9% yield). ^{1}H NMR (400 MHz, $CDCl_3$, TMS): δ = 0.89 (t, 3H, J = 7.6 Hz), 1.69–1.89 (m., 26H), 2.33 (s, 2H), 3.55 (s, 1H), 4.28 (t, 1H, J = 7.0 Hz). *(b) Propyloctamethylferrocene.* A solution of $BH_3{\cdot}SMe_2$ (6.3 mmol) in THF (3.0 mL, 2 M solution) was added to a stirred solution of 1-hydroxypropyloctamethylferrocene (0.320 g, 0.90 mmol) in THF (15 mL). After refluxing the solution for 1 h, the reaction was quenched with aqueous NH_4Cl (20 mL), and the solution extracted with CH_2Cl_2. The organic layer was dried over magnesium sulfate and concentrated under reduced pressure. The crude product was purified by column chromatography (alumina, pentane). The product was obtained as a yellow oil (0.253 g, yield 82.8%). ^{1}H NMR (400 MHz, $CDCl_3$, TMS): δ = 0.90 (t, 3H, J = 7.6 Hz), 1.29 (q, 4H, J = 7.5 Hz), 1.65–1.73 (br, 24H), 2.17 (t, 2H, J = 7.4 Hz), 3.21 (s, 1H).

The other alkyloctamethylferrocenes were prepared in a similar manner, and *trans*-1-pentenyloctamethylferrocene was obtained by dehydration of 1-hydroxypentyloctamethylferrocene (see ESI†).

Preparation of Tf_2N salts

[C3Fc][Tf$_2$N]. In the dark, $AgTf_2N$ (0.232 g, 0.60 mmol) was added to a solution of propyloctamethylferrocene (0.200 g, 0.59 mmol) in CH_2Cl_2 (10 mL). After stirring the solution for a few minutes, the mixture was filtered via a syringe equipped with a membrane filter to remove silver deposits and unreacted $AgTf_2N$. Removal of the solvent from the filtrate under reduced pressure gave the product as a dark-green solid (0.336 g, 92% yield), which was recrystallized from ethanol/hexane.

Dark-green plate crystals. Anal. Calcd (%) for $C_{23}H_{32}F_6FeNO_4S_2$ (620.47): C, 44.52; H, 5.20; N, 2.26. Found: C, 44.58; H, 5.23; N, 2.32. The other Tf_2N salts were prepared in a similar manner. For the purification of [**C10Fc**][Tf_2N] and [**C12Fc**][Tf_2N], they were dissolved in methanol and washed repeatedly with hexane to remove impurities. The solvents were evaporated under reduced pressure, and the residue was dried under vacuum at 80 °C for one day. ***[C5Fc][Tf_2N]***. Dark-green oil, 99% yield. Anal. Calcd (%) for $C_{25}H_{36}F_6FeNS_2O_4$ (648.53): C, 46.30; H, 5.60; N, 2.16. Found: C, 46.51; H, 5.74; N, 2.13. ***[C5'Fc][Tf_2N]***. Dark-green powder, 79% yield. Anal. Calcd (%) for $C_{25}H_{34}F_6FeNO_4S_2$ (646.51): C, 46.44; H, 5.30; N, 2.17. Found: C, 46.54; H, 5.39; N, 2.26. ***[C6Fc][Tf_2N]***. Dark-green oil, 95% yield. Anal. Calcd (%) for $C_{26}H_{38}F_6FeNO_4S_2$ (662.55): C, 47.13; H, 5.78; N, 2.11. Found: C, 47.27; H, 5.87; N, 2.13. ***[C8Fc][Tf_2N]***. Dark-green oil, 98% yield. Anal. Calcd (%) for $C_{28}H_{42}F_6FeNO_4S_2$ (690.60): C, 48.70; H, 6.13; N, 2.03. Found: C, 48.52; H, 6.18; N, 2.13. ***[C10Fc][Tf_2N]***. Dark-green oil, 68.3% yield (total yield from octamethylferrocene). Anal. Calcd (%) for $C_{30}H_{46}F_6FeNO_4S_2$ (718.66): C, 50.14; H, 6.45; N, 1.95. Found: C, 49.91; H, 6.55; N, 2.02. ***[C12Fc][Tf_2N]***. Dark-green solid, 92% yield. Anal. Calcd (%) for $C_{32}H_{50}F_6FeNO_4S_2$ (746.71): C, 51.47; H, 6.75; N, 1.88. Found: C, 51.44; H, 6.58; N, 1.98. ***[C17Fc][Tf_2N]***. Dark-green solid, 38.3% yield (total yield from octamethylferrocene). Anal. Calcd (%) for $C_{37}H_{60}F_6FeNO_4S_2$ (816.84): C, 54.40; H, 7.40; N, 1.71. Found: C, 54.18; H, 7.46; N, 1.96.

Preparation of PF_6 salts

[C4Fc][PF_6]. In the dark, a solution of $AgPF_6$ (51 mg, 0.20 mmol) in acetone (5 mL) was added to a solution of butyloctamethylferrocene (55 mg, 0.16 mmol) in acetone (10 mL). After stirring the solution for a few minutes, the mixture was filtered via a syringe equipped with a membrane filter to remove silver deposits and unreacted $AgPF_6$. Removal of the solvent from the filtrate under reduced pressure gave a solid, which was dissolved in CH_2Cl_2 (10 mL) and washed with water. After drying the organic

phase over magnesium sulfate, removal of the solvent gave the product as a dark-green solid (57 mg, 74% yield), which was recrystallized from ethanol (–50 °C). Green plate crystals. Anal. Calcd (%) for $C_{22}H_{34}FeF_6P$ (499.31): C, 52.62; H, 6.72. Found: C, 52.92; H, 6.86. The other PF_6 salts were prepared in a similar manner to that described above. ***[C6Fc][PF$_6$]***. Green plate crystals, 93% yield. Anal. Calcd (%) for $C_{24}H_{38}FeF_6P$ (527.37): C, 54.66; H, 7.26. Found: C, 54.45; H, 7.26. ***[C10Fc][PF$_6$]***. Green plate crystals, 63.3% yield. To remove impurities, the product was dissolved in methanol and washed repeatedly with hexane. Anal. Calcd (%) for $C_{28}H_{46}FeF_6P$ (583.47): C, 57.67; H, 7.95. Found: C, 57.35; H, 7.79.

Preparation of NO_3 salts

[C6Fc][NO$_3$]. In the dark, a solution of $AgNO_3$ (32 mg, 0.18 mmol) in water (2 mL) was added to a solution of hexyloctamethylferrocene (50 mg, 0.13 mmol) in acetone (2 mL) under stirring. After stirring for a few minutes, silver deposits and unreacted $AgNO_3$ were removed by filtration. The solvent was evaporated under reduced pressure, and the residue was dissolved in CH_2Cl_2 (50 mL) and washed with water (50 mL). The organic layer was dried over magnesium sulfate, and evaporation of the solvent under reduced pressure gave the product as a green powder in 85% yield; it was recrystallized from acetone/ether/pentane (1:30:70). Green plate crystals. Anal. Calcd (%) for $C_{24}H_{36}FeNO_3$ (444.22): C, 64.86; H, 8.62; N, 3.15. Found: C, 64.52; H, 8.62; N, 3.24. The other nitrate salts were prepared in a similar manner. ***[C10Fc][NO$_3$]***. Green powder, 48% yield from octamethylferrocene. To remove impurities, the product was dissolved in methanol and washed repeatedly with hexane. The solvent was evaporated under reduced pressure, and the residue was dried under vacuum at 80 °C for one day. Anal. Calcd (%) for $C_{28}H_{46}FeNO_3$ (500.51): C, 67.19; H, 9.26; N, 2.80. Found: C, 66.01; H, 9.07; N, 2.74. Recrystallization from acetone/ether/pentane (1:30:70) gave a small amount of single crystals.

Magnetic measurements

Magnetic measurements were carried out using a Quantum Design MPMS-XL7 SQUID susceptometer; 30–60 mg of samples were loaded in a quartz tube and used for the measurements. Samples of [**C4Fc**][Tf_2N] in confined spaces were prepared as follows. A glass capillary (inner diameter 0.2 mm, outer diameter 0.3–0.4 mm) was filled with a liquid sample of [**C4Fc**][Tf_2N] (11 mg), and cut into lengths of 5 mm. The short capillary-tubes were aligned and loaded into a quartz tube for SQUID measurements. To prepare thin-layer samples of thickness 25 μm, a liquid sample of [**C4Fc**][Tf_2N] was loaded into a quartz sample-tube, in which 200 sheets of spacers and separators prepared from copper TEM grids (diameter 3 mm, thickness 25 μm) were alternately carefully immersed. The magnetic susceptibility data were corrected for the diamagnetic contribution so that the χT values became constant in the high-temperature region. The data for [**C4Fc**][Tf_2N] and [**C5'Fc**][Tf_2N] were further corrected for a very small amount of ferromagnetic impurities (3×10^{-5} emu) from the magnetization curve.

X-ray structure determination

Single crystals for X-ray structure determination were obtained by recrystallization. [**C3Fc**][Tf_2N] was recrystallized from ethanol at –14 °C, and [**C4Fc**][PF_6], [**C6Fc**][PF_6], and [**C10Fc**][PF_6] from ethanol at –50 °C. [**C6Fc**][NO_3] and [**C10Fc**][NO_3] were obtained by slow diffusion of ether/pentane into acetone solutions (acetone : ether : pentane = 1:30:70). XRD data were collected with a Bruker Smart1000 CCD diffractometer using Mo Kα radiation (λ = 0.71073 Å) at –100 °C (cooling rate: 1 °C min^{-1}). The structures were solved by direct methods and refined using SHELXTL.[32] The crystallographic data are listed in Table 3. The crystallographic data for the structures have been deposited with the Cambridge Crystallographic Data Centre assupplementary publication nos. 900446 ([**C3Fc**][Tf_2N]), 900447

([**C4Fc**][PF_6]), 900448 ([**C6Fc**][PF_6]), 900449 ([**C6Fc**][NO_3]), 900450 ([**C10Fc**][PF_6]), and 900451 ([**C10Fc**][NO_3]).

Table 3. Crystallographic parameters for [**C3Fc**][Tf_2N], [**C4Fc**][PF_6], [**C6Fc**][PF_6], [**C6Fc**][NO_3], [**C10Fc**][PF_6], and [**C10Fc**][NO_3].

	[**C3Fc**][Tf_2N]	[**C4Fc**][PF_6]	[**C6Fc**][PF_6]	[**C6Fc**][NO_3]	[**C10Fc**][PF_6]	[**C10Fc**][NO_3]
Empirical formula	$C_{23}H_{32}F_6FeNO_4S_2$	$C_{22}H_{34}F_6FeP$	$C_{24}H_{38}F_6FeP$	$C_{24}H_{38}FeNO_3$	$C_{28}H_{46}F_6FeP$	$C_{28}H_{46}F_6FeP$
Formula weight	620.49	499.31	527.36	444.40	583.47	500.51
Crystal system	Monoclinic	Triclinic	Monoclinic	Monoclinic	Monoclinic	Triclinic
Space group	*C*2/*c* (No. 15)	*P*–1 (No. 2)	$P2_1/c$ (No. 14)	$P2_1/c$ (No. 14)	$P2_1/c$ (No. 14)	*P*–1 (No. 2)
a / Å	16.389(3)	12.6489(14)	16.0571(16)	17.982(5)	19.6648(18)	8.0742(13)
b / Å	18.944(3)	13.2409(15)	8.9074(9)	8.762(2)	8.7837(8)	9.8377(16)
c / Å	19.262(3)	13.8307(16)	17.6910(18)	17.319(5)	17.5494(16)	17.596(3)
α / °		91.767(2)				90.473(2)
β / °	113.192(2)	91.233(2)	96.246(2)	115.567(4)	102.498(2)	92.713(3)
γ / °		94.617(2)				97.649(3)
Volume / Å^3	5497.1(16)	2307.1(5)	2515.3(4)	2461.6(11)	2959.5(5)	1385.5(4)
Z	8	4	4	4	4	2
d_{calcd} / g cm^{-3}	1.499	1.438	1.393	1.199	1.310	1.201
μ / mm^{-1}	0.771	0.777	0.717	0.635	0.616	0.572
Reflections collected	14 381	12 027	12 924	11 578	15520	6926
Independent reflections	5195	8005	4741	4324	5600	4763
F(000)	2568	1044	1108	956	1236	542
Parameters	343	595	298	271	334	307
R_1[a], wR_2[b] ($I > 2\sigma$(I))	0.0390, 0.1087	0.0400, 0.1055	0.0641, 0.1901	0.0584, 0.1196	0.0392, 0.1061	0.0349, 0.1051
R_1[a], wR_2[b] (all data)	0.0447, 0.1135	0.0511, 0.1133	0.0772, 0.2038	0.0808, 0.1296	0.0546, 0.1175	0.0403, 0.1083
Goodness-of-fit on F^2	1.068	1.040	1.050	0.972	1.032	1.091

[a] $R_1 = \Sigma||F_o| - |F_c||/\Sigma\,|F_o|$. [b] $wR_2 = [\Sigma w(F_o^2 - F_c^2)^2/\Sigma w(F_o^2)^2]^{1/2}$.

Acknowledgement

This work was supported by KAKENHI (No. 24350073) from JSPS and the IMS (Institute for Molecular Science) Joint Studies Program. We thank Dr. Yoshito Furuie (Kobe University) for elemental analyses and Masaru Nakama (Crayonsoft Inc.) for providing a Web-DB system.

Notes and references

[a] *Department of Chemistry, Graduate School of Science, Kobe University, Rokkodai, Nada, Hyogo 657-8501, Japan. E-mail: tmochida@platinum.kobe-u.ac.jp*

[b] *Center for Supports to Research and Education Activities, Kobe University, Rokkodai, Nada, Hyogo 657-8501, Japan*

[c] *Molecular Photoscience Research Center, Kobe University, Rokkodai, Nada, Hyogo 657-8501, Japan*

[d] *Institute for Molecular Science, Myodaiji, Okazaki, Aichi 444-8585, Japan*

† Electronic Supplementary Information (ESI) available: Preparation of alkyloctamethylferrocnes, results of the DSC, XRD, and magnetic measurements. See DOI: 10.1039/b000000x/

‡ Present address: Center for Instrumental Analysis, Institute for Research Promotion, Niigata University, Nishi-ku, Niigata 950-2181, Japan

1 (*a*) *Ionic Liquid: Industrial Applications to Green Chemistry*, Eds. R. D. Rogers and K. R.Seddon, ACS Symposium Series, American Chemical Society, Washington, D. C., 2002, Vol. *818*; (*b*) A. Stark and K. R. Seddon, In *Kirk-Othmer Encyclopedia of Chemical Technology*, 5th ed. Wiley-Interscience, New York, 2007, Vol. *26*, pp 836–919; (*c*) M. Armand, F. Endres, D. R. MacFarlane, H. Ohno and B. Scrosati, *Nat. Mater.*, 2009, **8**, 621–629; (*d*) I. Krossing, J. M. Slattery, C. Daguenet, P. J. Dyson, A. Oleinikova and H. Weingärtner, *J. Am. Chem. Soc.*, 2006, **128**, 13427–13434; (*e*) H. Weingärtner, *Angew. Chem. Int. Ed.* 2008, **47**, 654–670; (*f*) Y. Yoshida and G. Saito, *Phys. Chem. Chem. Phys.*, 2010, **12**, 1675–1684.

2 (*a*) J. H. Davis, Jr., *Chem. Lett.*, 2004, **33**, 1072–1077; (*b*) S. -G. Lee, *Chem. Commun.*, 2006, 1049–1063; (*c*) M. Pucheault and M. Vaultier, *Top. Curr. Chem.*, 2010, **290**, 83–126; (*d*) A. D. Sawant, D. G. Raut, N. B. Darvatkar and M. M. Salunkhe, *Green Chem. Lett. Rev.*, 2011, **4**, 41–54.

3 (*a*) S. Hayashi and H. Hamaguchi, *Chem. Lett.,* 2004, **33**, 1590–1591; (*b*) Y. Yoshida, A. Otsuka, G. Saito, S. Natsume, E. Nishibori, M. Takata, M. Sakata, M. Takahashi and T. Yoko, *Bull.*

Chem. Soc. Jpn., 2005, **78**, 1921–1928; (*c*) P. Nockemann, B. Thijs, N. Postelmans, K. Van Hecke, L. Van Meervelt and K. Binnemans, *J. Am. Chem. Soc.*, 2006, **128**, 13658–13589; (*d*) B. Mallick, B. Balke, C. Felser and A. -V. Mudring, *Angew. Chem., Int. Ed*., 2008, **47**, 7635–7638; (*e*) T. Peppel, M. Köckerling, M. Geppert-Rybczyńska, R. V. Ralys, J. K. Lehmann, S. P. Verevkin and A. Heintz, *Angew. Chem., Int. Ed*., 2010, **49**, 7116–7119; (*f*) B. M. Krieger, H. Y. Lee, T. J. Emge, J. F. Wishart and E. W. Castner, Jr., *Phys. Chem. Chem. Phys*., 2010, **12**, 8919–8925.

4 Y. Yoshida, H. Tanaka and G. Saito, *Chem. Lett*., 2007, **36**, 1096–1097.

5 (*a*) R. E. Del Sesto, C. Corley, A. Robertson and J. Wilkes, *J. Organomet. Chem.*, 2005, **690**, 2536–2542; (*b*) Y. Yoshida, H. Tanaka, G. Saito, L. Ouahab, H. Yoshida and N. Sato, *Inorg. Chem.*, 2009, **48**, 9989–9991; (*c*) A. Branco, L. C. Branco and F. Pina, *Chem. Commun.*, 2011, 2300–2302; (*d*) P. Zhang, Y. Gong, Y. Lv, Y. Guo, Y. Wang, C. Wang and H. Li, *Chem. Commun.*, 2012, **48**, 2334–2336.

6 (*a*) H. Masui and R. W. Murray, *Inorg. Chem.*, 1997, **36**, 5118–5126; (*b*) J. F. Huang, H. M. Luo and S. Dai, *J. Electrochem. Soc.*, 2006, **153**, J9–J13; (*c*) M. D. Lequerica, M. J. Baena and P. Espinet, *Inorg. Chim. Acta*, 2008, **361**, 2270–2278; (*d*) M. Iida, C. Baba, M. Inoue, H. Yoshida, E. Taguchi and H. Furusho, *Chem. Eur. J*., 2008, **14**, 5047–5056; (*e*) T. Tamura, K. Yoshida, T. Hachida, M. Tsuchiya, M. Nakamura, Y. Kazue, N. Tachikawa, K. Dokko and M. Watanabe, *Chem. Lett.*, 2010, **39**, 753–755; (*f*) T. M. Anderson, D. Ingersoll, A. J. Rose, C. L. Staiger and J. C. Leonard, *Dalton Trans.*, 2010, **39**, 8609–8612; (*g*) Y. Song, H. Jing, B. Li and D. Bai, *Chem. Eur. J.*, 2011, **17**, 8731–8738; (*h*) N. R. Brooks, S. Schaltin, K. Van Hecke, L. Van Meervelt, K. Binnemans and J. Fransaer, *Chem. Eur. J.*, 2011, **17**, 5054–5059; (*i*) S. Schaltin, N. R. Brooks, L.

Stappers, K. Van Hecke, L. Van Meervelt, K. Binnemans and J. Fransaer, *Phys. Chem. Chem. Phys.*, 2012, **14**, 1706–1715.

7 (*a*) T. Inagaki and T. Mochida, *Chem. Lett.*, 2010, **39**, 572–573; (*b*) Y. Funasako, T. Mochida, T. Inagaki, T. Sakurai, H. Ohta, K. Furukawa and T. Nakamura, *Chem. Commun.*, 2011, **47**, 4475–4477; (*c*) Y. Funasako, K. Abe and T. Mochida, *Thermochim. Acta*, 2012, **532**, 78–82; (*d*) T. Inagaki, T. Mochida, M. Takahashi, C. Kanadani, T. Saito and D. Kuwahara, *Chem. Eur. J.*, 2012, **18**, 6795–6804; (*e*) T. Inagaki and T. Mochida, *Chem. Eur. J.*, 2012, **18**, 8070–8075; (*f*) S. Mori, T. Mochida, *Organometallics*, 2013, **32**, 780–787.

8 (*a*) Y. Funasako, T. Mochida, K. Takahashi, T. Sakurai and H. Ohta, *Chem. Eur. J.*, 2012, **18**, 11929–11936; (b) M. Okuhata and T. Mochida, *Polyhedron*, 2012, **43**, 153–158.

9 (*a*) *Ferrocenes: Homogenous Catalysis, Organic Synthesis, Materials Science*, Eds. A. Togni and T. Hayashi, Wiley-VCH, Weinheim, 1995, Chapter 8, and references therein; (*b*) D. De Caro, C. Faulmann and L. Valade, *Chem. Eur. J.*, 2007, **13**, 1650–1663; (*c*) J. S. Miller, A. J. Epstein and W. M. Reiff, *Angew. Chem., Int. Ed. Engl.*, 1994, **33**, 385–415; (*d*) J. S. Miller, *J. Mater. Chem.*, 2010, **20**, 1846–1857.

10 S. Ulrich, *Polyhedron*, 1997, **16**, 1513–1516.

11 (*a*) R. Deschenaux, M. Schweissguth and A. -M. Levelut, *Chem. Commun.*, 1996, 1275–1276; (*b*) R. Deschenaux, M. Schweissguth, M. -T. Vilches, A. -M. Levelut, D. Hautot, G. L. Long and D. Luneau, *Organometallics*, 1999, **18**, 5553–5559.

12 P. M. Dean, J. M. Pringle, D. R. MacFarlane, *Phys. Chem. Chem. Phys.*, 2010, **12**, 9144–9153.

13 T. Mochida and S. Saruta, unpublished result.

14 (*a*) N. V. Plechkova and K. R. Seddon, *Chem. Soc. Rev.*, 2008, **37**, 123–150; (*b*) H. Tokuda, K. Hayamizu, K. Ishii, M. A. B. H. Susan and M. Watanabe, *J. Chem. Phys. B*, 2005, **109**, 6103–6110.

15 D. Turnbull and M. H. Cohen, *Modern Aspect of the Vitreous State*, Butterworth, *Vol. 1*, London, 1960, p. 38.

16 O. Yamamuro, Y. Minamimoto, Y. Inamura, S. Hayashi and H. Hamaguchi, *Chem. Phys. Lett.*, 2006, **423** 371–375.

17 J. Timmermans, *J. Phys. Chem. Solids*, 1961, **18**, 1–8.

18 (*a*) Y. U. Paulechka, A. V. Blokhin, G. J. Kabo and A. A. Strechan, *J. Chem. Thermodyn.*, 2007, **39**, 866–877; (*b*) Y. Shimizu, Y. Ohte, Y. Yamamura and K. Saito, *Chem. Phys. Lett.*, 2009, **470**, 295–299.

19 A. Paul and A. Samanta, *J. Phys. Chem. B*, 2008, **112**, 16626–16632.

20 G. S. Fulcher, *J. Am. Ceram. Soc*., 1925, **8**, 339–355.

21 K. R. Harris, M. Kanakubo and L. A. Woolf, *J. Chem*. *Eng*. *Data*, 2007, **52**, 1080–1085.

22 C. A. Angell, *J. Non-Cryst. Solids*, 1985, **73**, 1–17.

23 H. Schottenberger, K. Wurst and R. H. Herber, *J. Organomet. Chem*. 2001, **625**, 200–207.

24 T. Mochida, Y. Funasako, T. Inagaki, M. -J. Li, K. Asahara and D. Kuwahara, in preparation.

25 J. S. Miller, D. T. Glatzhofer, D. M. O'Hare, W. M. Reiff, A. Chakraborty and A. J. Epstein, *Inorg. Chem.*, 1989, **28**, 2930–2939.

26 (*a*) P. De Rango, M. Lees, P. Lejay, A. Sulpice, R. Tournier, M. Ingold, P. Germi and M. Pernet, *Nature*, 1991, **349**, 770–772; (*b*) A. E. Mikelson and Y. K. Karklin, *J. Cryst. Growth*, 1981, **52**, 524–529; (*c*) T. Sugiyama, M. Tahashi, K. Sassa and S. Asai, *ISIJ Int.*, 2003, **43**, 855–861.

27 K. Nishimura and G. Saito, *Synth. Met.*, 2005, **153**, 385–388.

28 W. Fujita, K. Awaga, Y. Nakazawa, K. Saito and M. Sorai, *Chem. Phys. Lett.*, 2002, **352**, 348–352.

29 (*a*) Y. Galyametdinov, M. A. Athanassopoulou, K. Griesar, O. Kharitonova, E. A. Soto Bustamante, L. Tinchurina, I. Ovchinnikov and W. Haase, *Chem. Mater.*, 1996, **8**, 922–926; (*b*) K. Binnemans, Y. G. Galyametdinov, R. Van Deun, D. W. Bruce, S. R. Collinson, A. P. Polishchuk, I. Bikchantaev, W. Haase, A. V. Prosvirin, L. Tinchurina, I. Litvinov, A. Gubajdullin, A. Rakhmatullin, K. Uytterhoeven and L. Van Meervelt, *J. Am. Chem. Soc.*, 2000, **122**, 4335–4344.

30 C. Zou and M. S. Wrighton, *J. Am. Chem. Soc.*, 1990, **112**, 7578–7584.

31 A. Vij, Y. Y. Zheng, R. L. Kirchmeier and J. M. Shreeve, *Inorg. Chem.*, 1994, **33**, 3281–3288.

32 G. M. Sheldrick, *SHELXL: Program for the Solution for Crystal Structures*, University of Göttingen, Germany, 1997.

Figure Captions

Scheme 1 Structural formulae of alkyloctamethylferrocenium salts prepared in this study. Abbreviations for the salts are also shown.

Scheme 2 Scheme for preparation of alkyloctamethylferrocenium salts.

Fig. 1 Melting points of Tf_2N salts (●) and alkyloctamethylferrocenes (○) plotted as a function of the alkyl-chain length. The values for octamethylferrocene and its Tf_2N salt ($n = 0$) are also shown.

Fig. 2 Phase sequences of Tf_2N salts. Different crystal phases are represented as I–III. The asterisks indicate metastable phases.

Fig. 3 Schematic Gibbs free energy diagram for [**C5Fc**][Tf_2N]. The free energy curves are approximated by straight lines for simplicity.

Fig. 4 Sums of phase transition entropies of Tf_2N salts. The dark-gray areas are the entropies of solid phase transitions, and the others are the melting entropies.

Fig. 5 Packing diagrams of (a) [**C3Fc**][Tf_2N], (b) [**C4Fc**][PF_6], (c) [**C6Fc**][PF_6], (d) [**C6Fc**][NO_3], (e) [**C10Fc**][PF_6], and (f) [**C10Fc**][NO_3]. Hydrogen atoms have been omitted for clarity.

Fig. 6 Temperature dependence of the magnetic susceptibilities of [**C4Fc**][Tf_2N] in the form of a χT–T plot. The data measured under 0.5 T are shown by open circles, and those for a sample crystallized under a perpendicular field of 0.59 T are shown by filled circles (heating run).

Fig. 7 Angular dependence of ESR spectra recorded at intervals of 10°. Inset shows the angular dependences of g-value at –269.4 °C, measured on a sample of [**C4Fc**][Tf_2N] crystallized under a magnetic field of 0.8 T. θ is defined as the angle between the magnetic fields used for crystallization and ESR measurements.

Fig. 8 Temperature dependences of magnetic susceptibilities of [**C12Fc**][Tf_2N] in the form of χT–T plots, measured under 0.1 T (dotted line), 1 T (solid line), and 7 T (broken line) in the cooling processes.

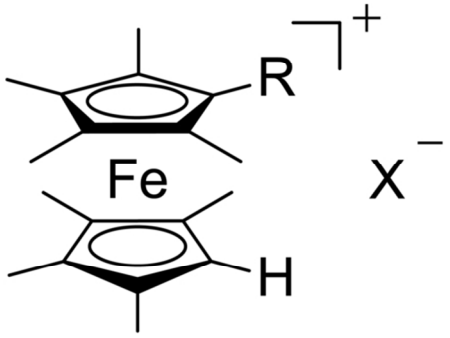

X = Tf_2N, PF_6, NO_3

salts	R
[**C3Fc**][X]	*n*-propyl
[**C4Fc**][X]	*n*-butyl
[**C5Fc**][X]	*n*-pentyl
[**C6Fc**][X]	*n*-hexyl
[**C8Fc**][X]	*n*-octyl
[**C10Fc**][X]	*n*-decyl
[**C12Fc**][X]	*n*-dodecyl
[**C17Fc**][X]	*n*-heptadecyl
[**C5'Fc**][X]	1-pentenyl

48x29mm (600 x 600 DPI)

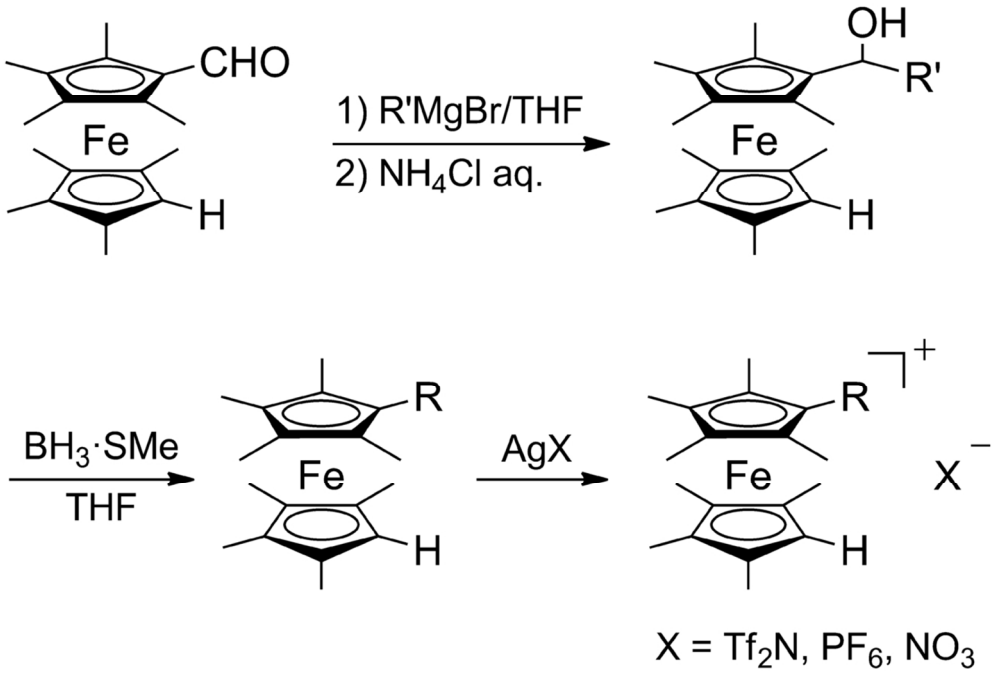

55x37mm (600 x 600 DPI)

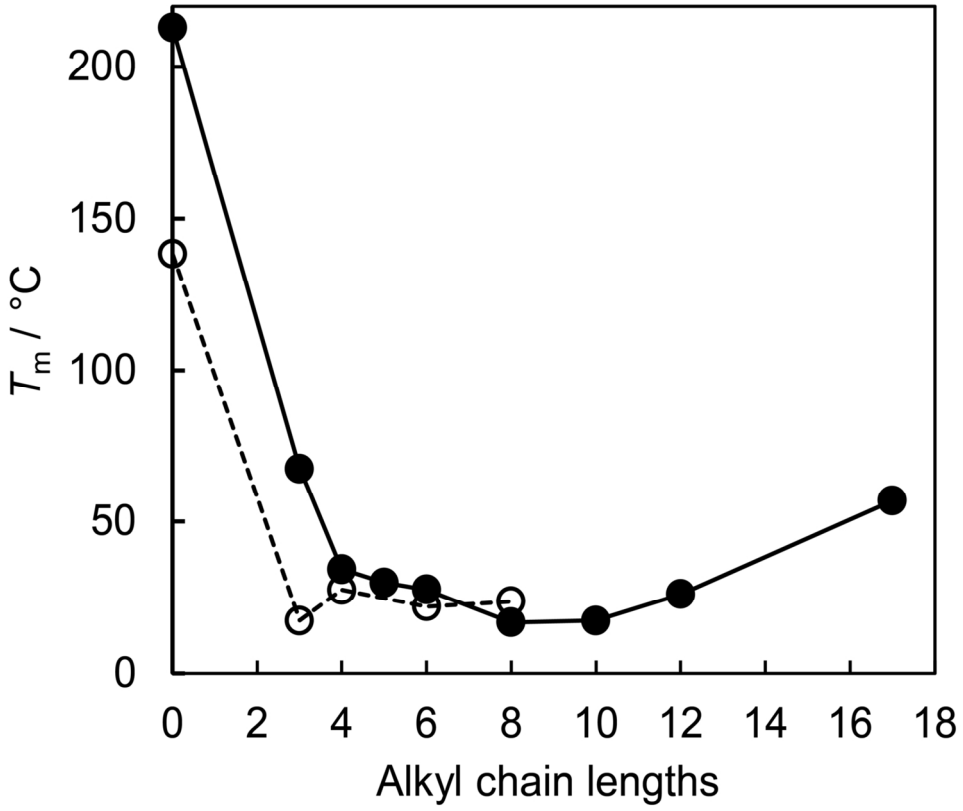

67x57mm (600 x 600 DPI)

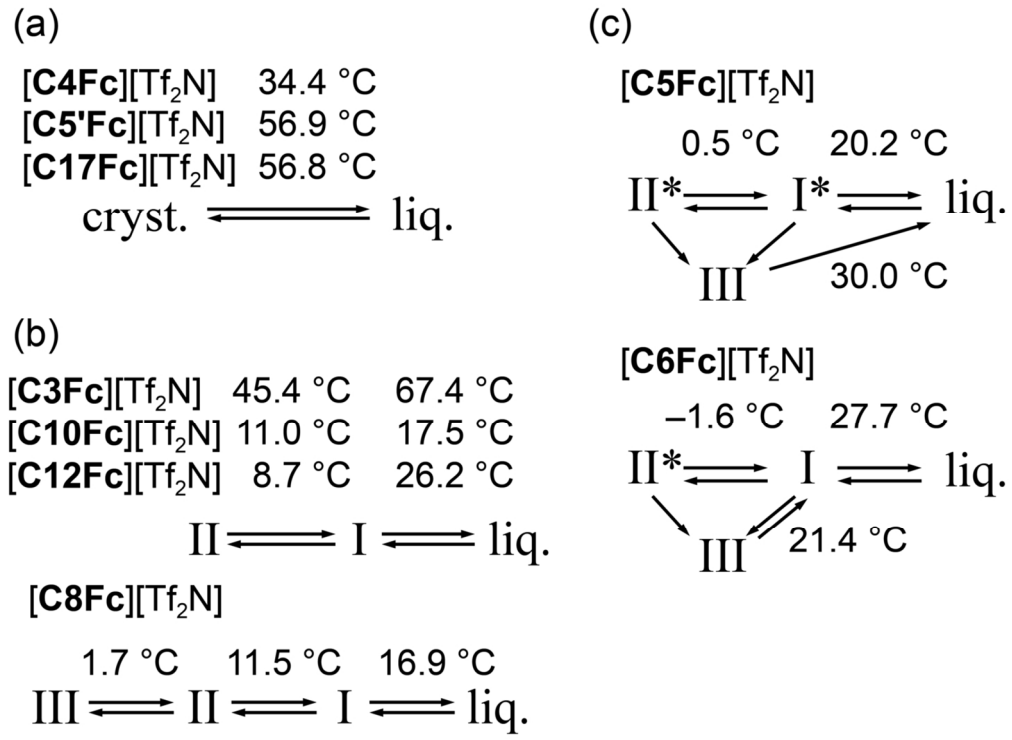

61x45mm (600 x 600 DPI)

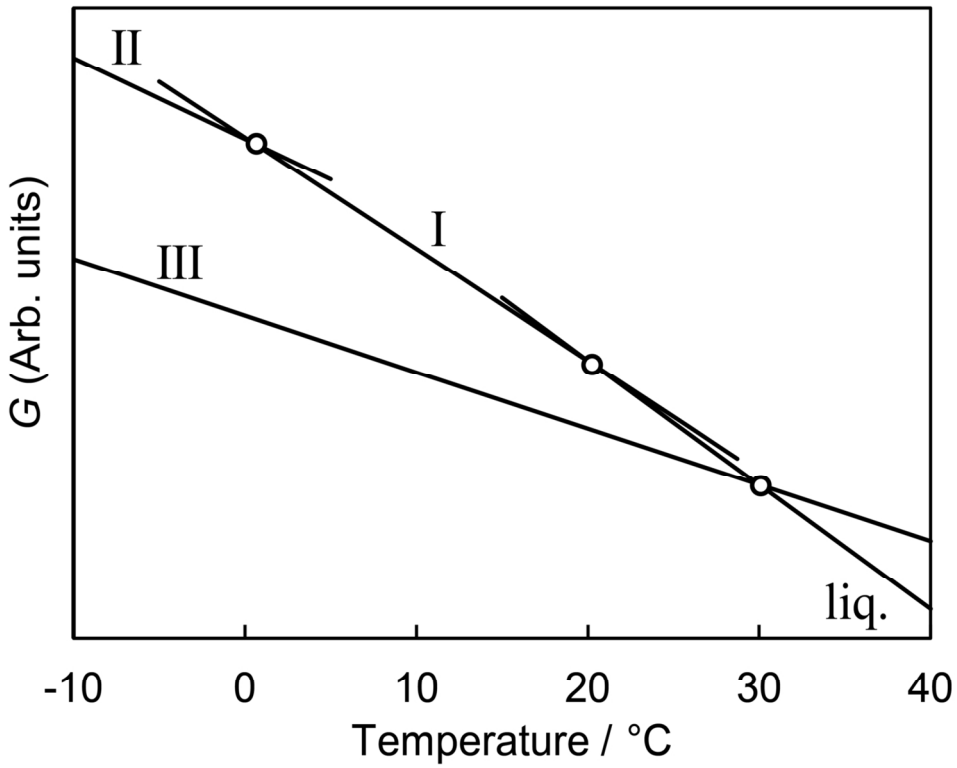

65x53mm (600 x 600 DPI)

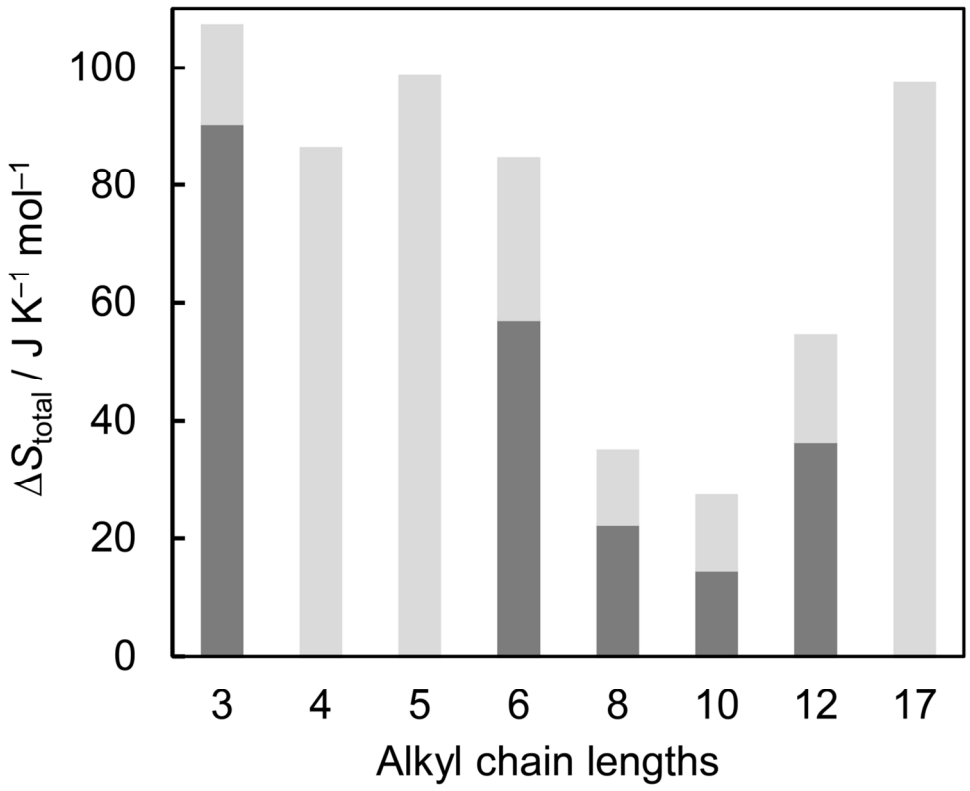

65x54mm (600 x 600 DPI)

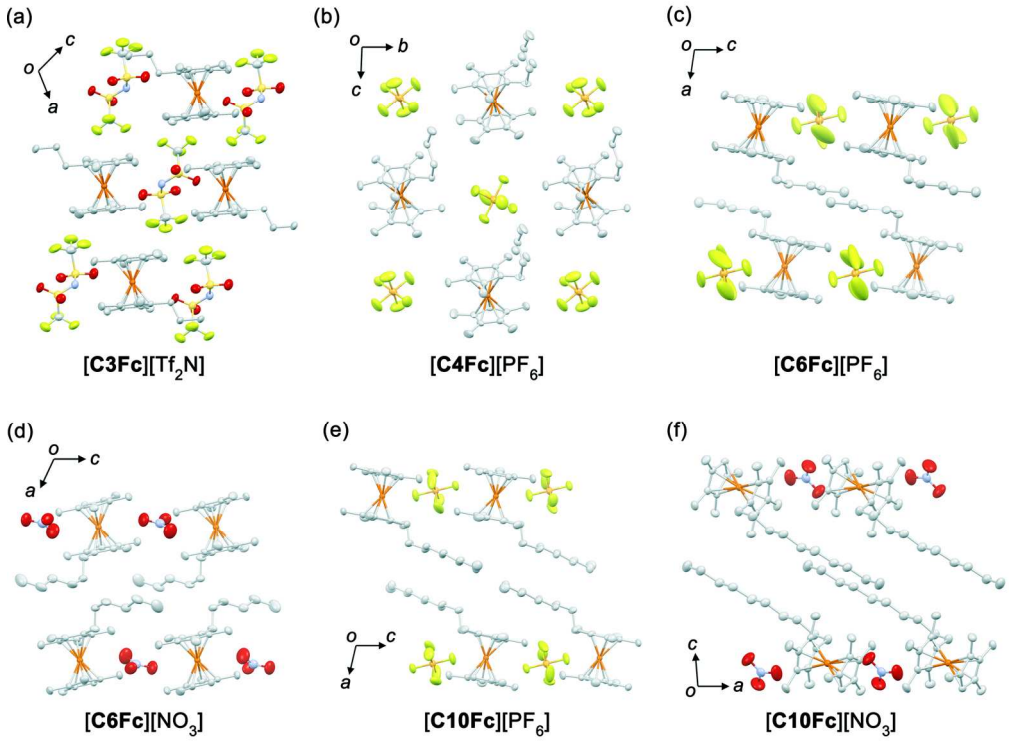

170x127mm (300 x 300 DPI)

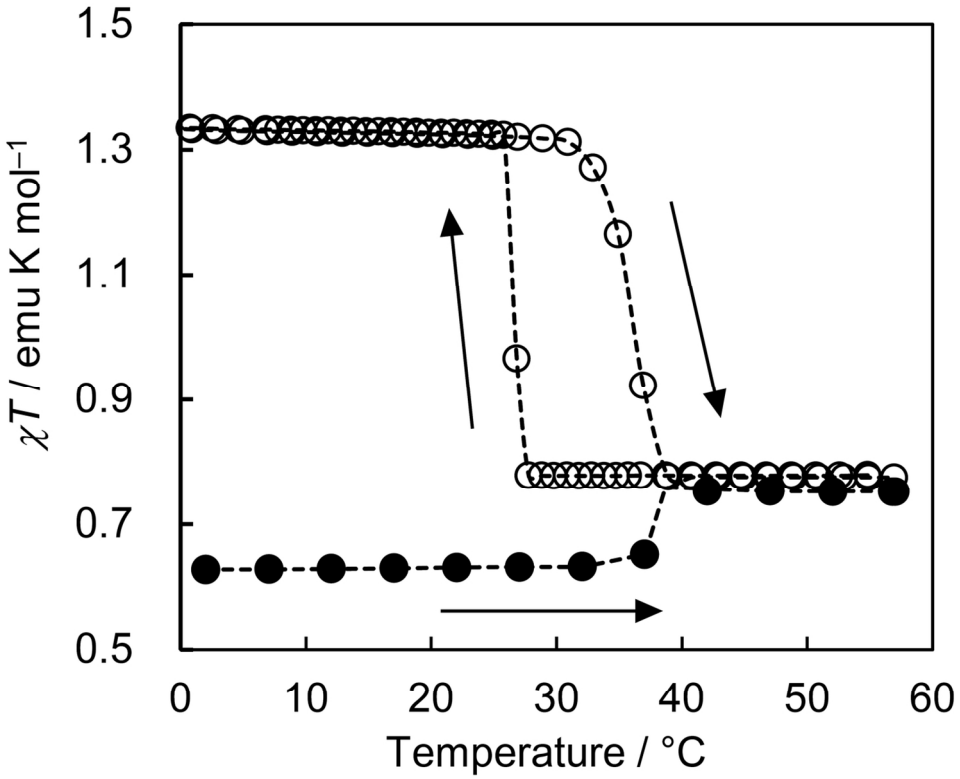

64x52mm (600 x 600 DPI)

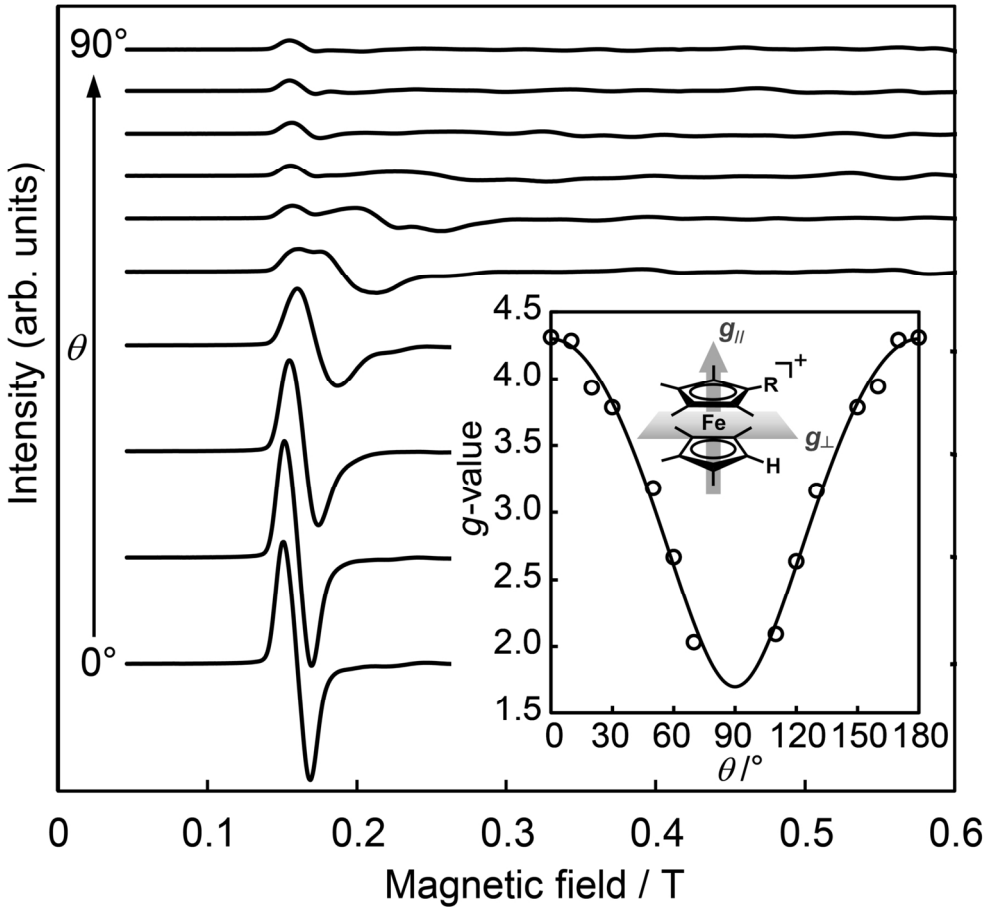

77x73mm (600 x 600 DPI)

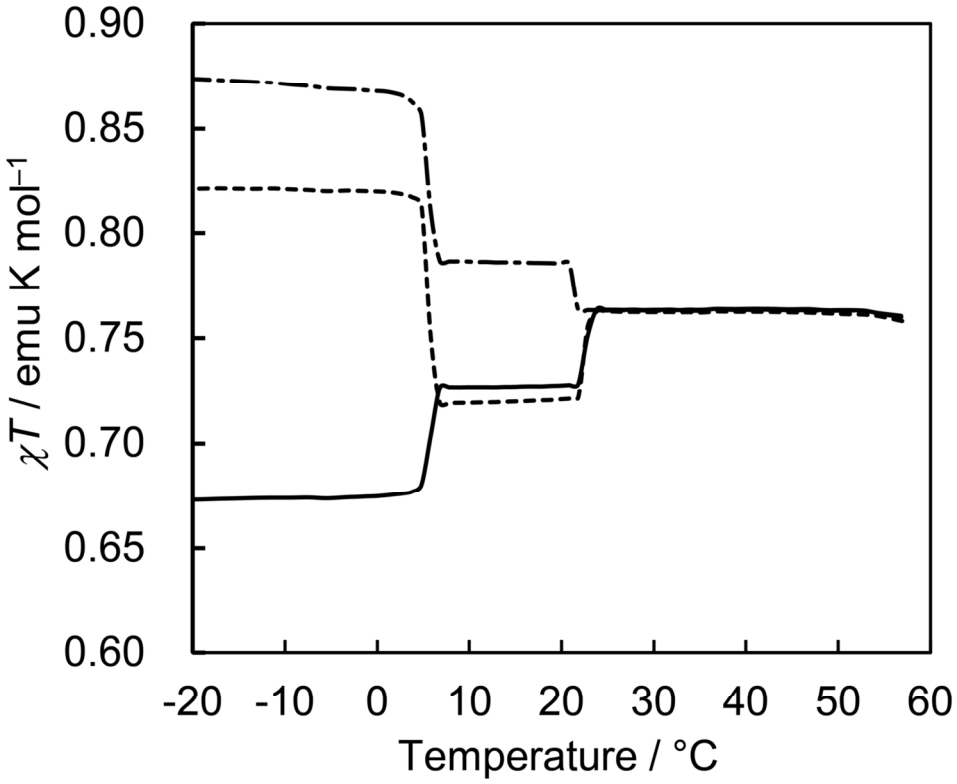

65x52mm (600 x 600 DPI)

Table of contents entry:

Organometallic Ionic Liquids from Alkyloctamethylferrocenium Cations: Thermal Properties, Crystal Structures, and Magnetic Properties

Yusuke Funasako[a], Takashi Inagaki[a], Tomoyuki Mochida,*[a] Toshihiro Sakurai[b], Hitoshi Ohta[c], Ko Furukawa[d] and Toshikazu Nakamura[d]

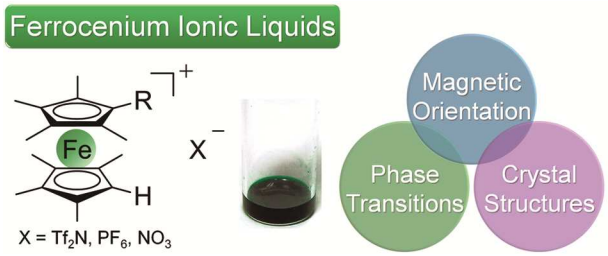

The thermal properties, viscosities, crystal structures, and magnetic properties of alkylferrocenium ionic liquids were investigated.

Electronic Supplementary Information

Organometallic Ionic Liquids from Octamethylferrocenium Cations: Preparation, Thermal Properties, Crystal Structures, and Magnetic Properties

Yusuke Funasako,[a] Takashi Inagaki,[a] Tomoyuki Mochida,*[a] Toshihiro Sakurai,[b] Hitoshi Ohta,[c] Ko Furukawa[d] and Toshikazu Nakamura[d]

[a]*Department of Chemistry, Graduate School of Science, Kobe University, Rokkodai, Nada, Hyogo 657-8501, Japan*

[b]*Center for Supports to Research and Education Activities, Kobe University, Rokkodai, Nada, Hyogo 657-8501, Japan*

[c]*Molecular Photoscience Research Center, Kobe University, Rokkodai, Nada, Hyogo 657-8501, Japan*

[d]*Institute for Molecular Science, Myodaiji, Okazaki, Aichi 444-8585, Japan*

1. Preparation of alkyloctamethylferrocenes

Alkyloctamethylferrocenes were prepared in a similar manner to that described for propyloctamethylferrocene in the text, and the data are shown below.

Pentyloctamethylferrocene: a) 1-Hydroxypentyloctamethylferrocene. Yellow-orange solid, 72.6% yield. b) Pentyloctamethylferrocene. Yellow oil, 64.5% yield. ^{1}H NMR (400 MHz, $CDCl_3$, TMS): δ = 0.88 (t, 3H, J = 6.8 Hz), 1.29 (br, 6H), 1.63–1.70 (br, 24H), 2.14 (s, 2H), 3.23 (s, 1H). Anal. Calcd (%) for $C_{23}H_{36}Fe$ (368.4): C, 74.99; H, 9.85. Found: C, 74.58; H, 9.96. **Hexyloctamethylferrocene:** a) 1-Hydroxyhexyloctamethylferrocene. Yellow solid, 90% yield. ^{1}H NMR (400 MHz, $CDCl_3$, TMS): δ = 0.87 (t, 3H, J = 6.8 Hz), 1.26 (br, 6H), 1.43 (br, 2H), 1.65–1.76 (m, 21H), 1.90 (s, 3H), 2.31 (s, 1H), 3.55 (s, 1H), 4.40 (br, 1H). b) Hexyloctamethylferrocene. Yellow oil, 90% yield. ^{1}H NMR (400 MHz, $CDCl_3$, TMS): δ = 0.87 (t, 3H, J = 6.8 Hz), 1.29 (br, 8H), 1.65 (s, 6H), 1.73 (m, 18H), 2.17 (t, 2H, J = 7.2 Hz), 3.20 (s, 1H). Anal. Calcd (%) for $C_{24}H_{38}Fe$ (382.4): C, 75.38; H, 10.02. Found: C, 75.39; H, 10.13. **Octyloctamethylferrocene:** a)

1-Hydroxyoctyloctamethylferrocene. Yellow solid, 76.5% yield. ^{1}H NMR (400 MHz, $CDCl_3$, TMS): δ = 0.88 (t, 3H, J = 6.8 Hz), 1.25 (br, 8H), 1.43 (br, 2H), 1.68–1.76 (m, 21H), 1.89 (s, 3H), 2.31 (s, 1H), 3.55 (s, 1H), 4.35 (br, 1H). b) Octyloctamethylferrocene. Yellow oil, 83% yield. ^{1}H NMR (400 MHz, $CDCl_3$, TMS): δ = 0.88 (t, 3H, J = 6.8 Hz), 1.26 (br, 12H), 1.66 (s, 6H), 1.73 (m, 18H), 2.18 (br, 2H), 3.21 (s, 1H). Anal. Calcd (%) for $C_{26}H_{42}Fe$ (382.4): C, 76.08; H, 10.31. Found: C, 76.01; H, 10.32. **Decyloctamethylferrocene:** a) 1-Hydroxydecyloctamethylferrocene. Yellow oil. ^{1}H NMR (400 MHz, $CDCl_3$, TMS): δ = 0.89 (t, 4.3H, J = 6.2 Hz), 1.26 (br, 18H), 1.43 (br, 2H), 1.69–1.76 (m, 21H), 1.89 (s, 3H), 2.31 (s, 1H), 3.55 (s, 1H), 4.35 (br, 1H). The crude product was used for the next step without purification. b) Decyloctamethylferrocene. Yellow oil. ^{1}H NMR (400 MHz, $CDCl_3$, TMS): δ = 0.88 (t, 4.4H, J = 6.8 Hz), 1.26 (br, 22H), 1.68 (s, 6H), 1.73 (m, 18H), 2.18 (t, 2H, J = 7.4 Hz), 3.20 (s, 1H). The crude product was used for the salt preparation without purification. **Dodecyloctamethylferrocene:** a) 1-Hydroxydodecyloctamethylferrocene. Yellow solid, 48.5% yield (crude). The crude product was used for the next step without purification. b) Dodecyloctamethylferrocene. Yellow oil, 71% yield (crude). ^{1}H NMR (400 MHz, $CDCl_3$, TMS): δ = 0.88 (t, 3.4H, J = 6.8 Hz), 1.25 (br, 22H), 1.63–1.70 (m, 24H), 2.14 (br, 2H), 3.22 (s, 1H). The crude product was used for the salt preparation without purification. **Heptadecyloctamethylferrocene:** a) 1-Hydroxyheptadecyloctamethylferrocene. Yellow solid. The crude product was used for the next step without purification. b) Heptadecyloctamethylferrocene. Yellow oil. The crude product was used for the salt preparation without purification. ***trans*-1-Pentenyloctamethylferrocene:** 1-Hydroxypentyloctamethylferrocene (0.531 g), prepared similarly, was distilled under vacuum at 130 °C to give the product within an hour as a dark-brown oil (0.268 g, 53%). ^{1}H NMR (400 MHz, $CDCl_3$, TMS): δ = 0.94 (m, 3H), 1.47 (m, 2H), 1.65 (s, 6H), 1.70 (s, 6H), 1.77 (s, 6H), 1.86 (s, 6H), 2.11 (m 2H), 3.55 (s, 1H), 5.87 (m, 1H), 6.04 (d, 1H, J = 16.0 Hz). Anal. Calcd (%) for $C_{23}H_{34}Fe$ (354.4): C, 75.40; H, 9.35. Found: C, 75.34; H, 9.44.

2. Thermal behavior of [C5Fc][Tf_2N]

The DSC trace of [**C5Fc**][Tf_2N] is shown in Figure S1. When cooled from the melt, crystallization occurred at around –2.3 °C to give phase I, and with further cooling, a phase transition to phase II occurred at around –11.5 °C (ΔS = 44.2 J K^{-1} mol^{-1}). In the heating run, phase I melted at 20.2 °C (Figure S1c), but an unprecedented, exothermal transition to phase III often occurred (Figures S1a and S1b). In the heating run, a transition from phase II to III occurred at –8.5 °C (Figure S1a). In the run shown in Figure S1b, a transition from phase II to I occurred at 0.4 °C, followed by an exothermal transition to phase III, which melted at 30.0 °C.

3. Figures

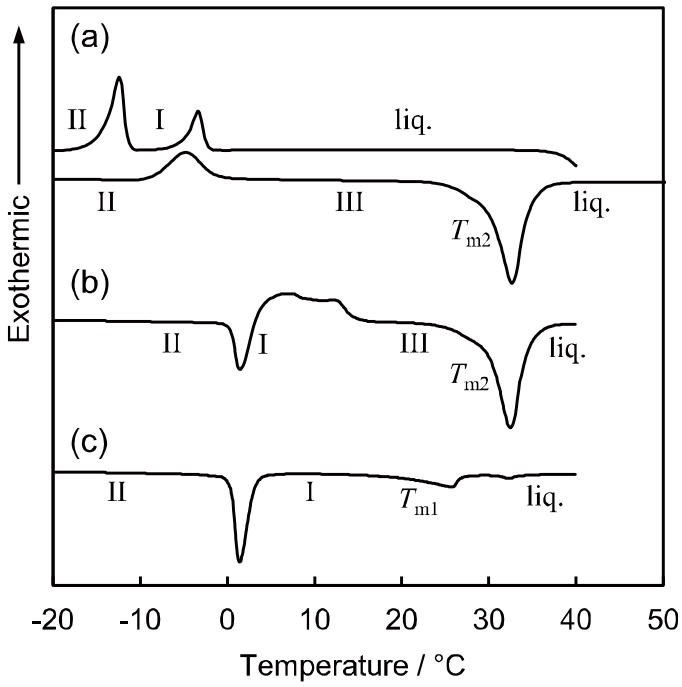

Fig. S1 DSC traces of [pentyloctamethylferrocenium][Tf_2N] ([**C5Fc**][Tf_2N]) measured at 10 °C min^{-1}. Only the heating runs are shown in (b) and (c).

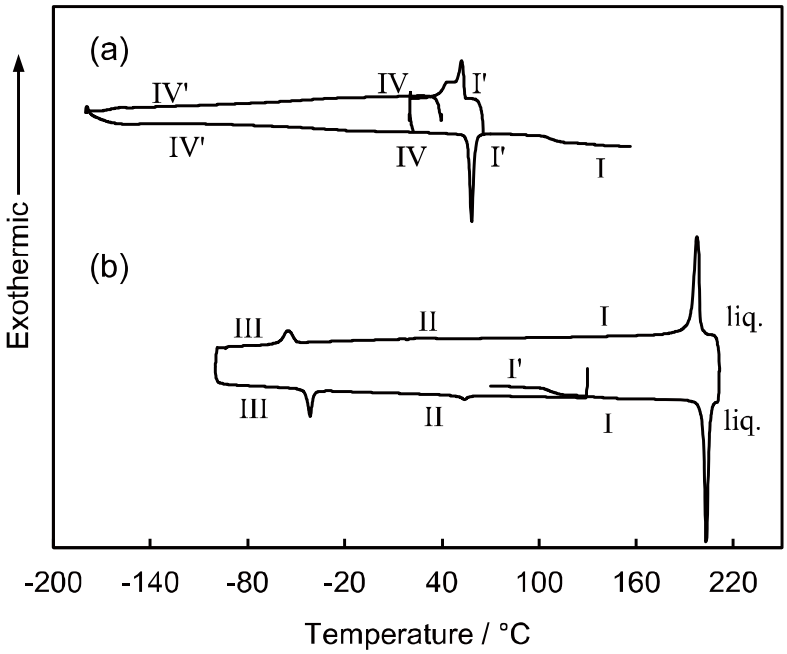

Fig. S2 DSC traces of [decyloctamethylferrocenium][PF_6] ([**C10Fc**][PF_6]) measured at 10 °C min^{-1}. Cycles (a) before and (b) after experiencing glass transition from phase I' to phase I are shown.

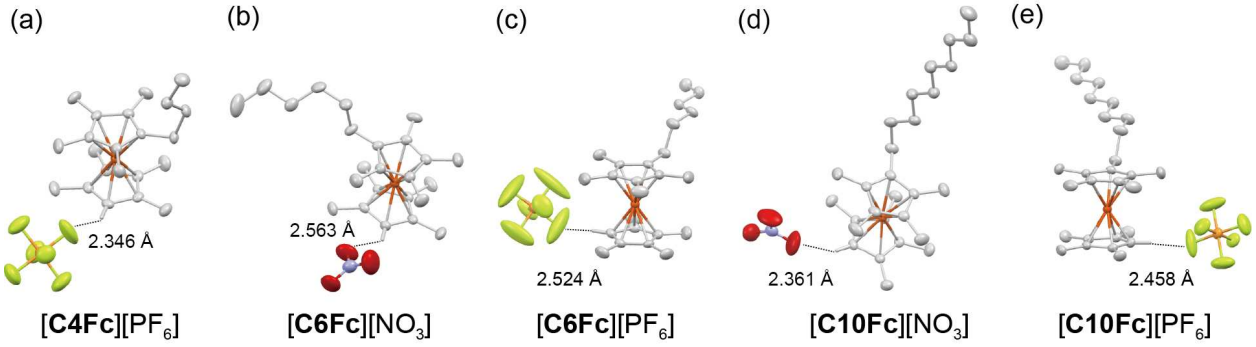

Fig. S3 Molecular structures of (a) [**C4Fc**][PF_6], (b) [**C6Fc**][NO_3], (c) [**C6Fc**][PF_6], (d) [**C10Fc**][NO_3], and (e) [**C10Fc**][PF_6]. C–H...X contacts are indicated by dotted lines.

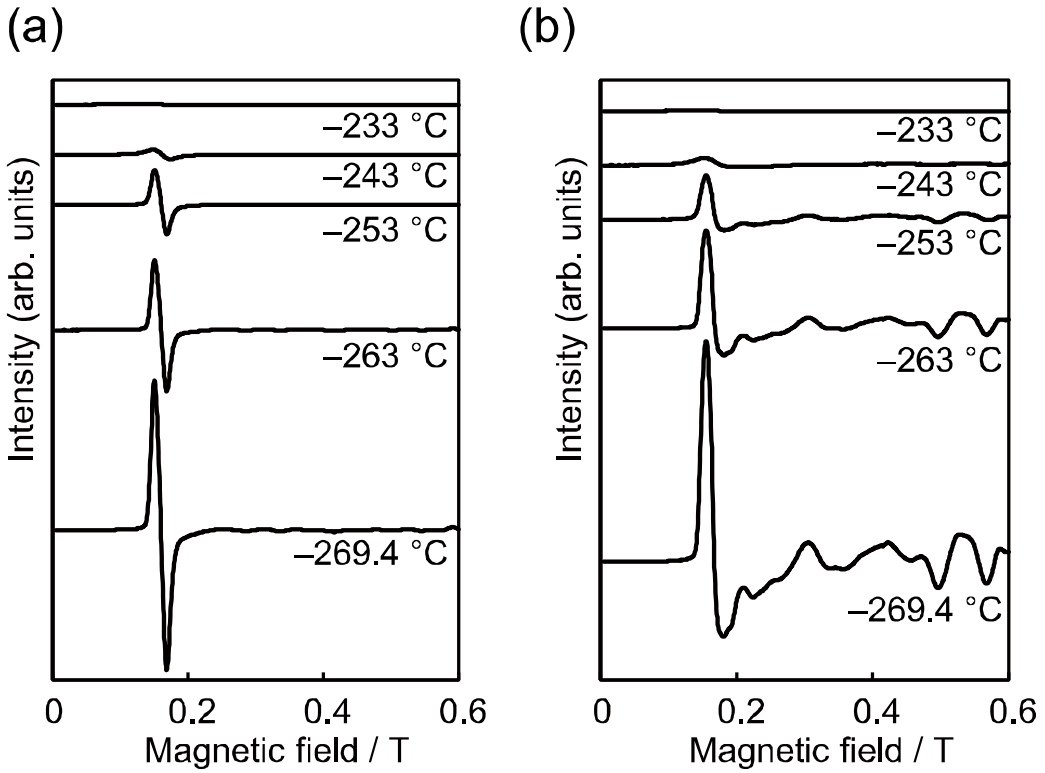

Fig. S4 Temperature dependences of ESR spectra of [**C4Fc**][Tf_2N] crystallized (a) under a magnetic field of 0.8 T and (b) without a magnetic field.

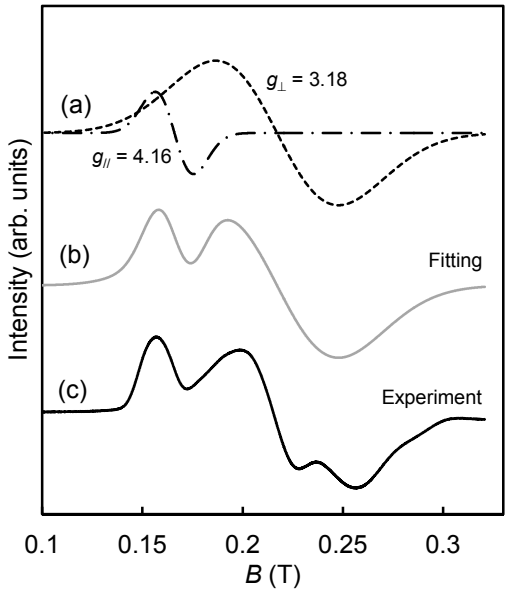

Fig. S5 (a) ESR spectra of [**C4Fc**][Tf_2N] crystallized under a magnetic field of 0.8 T recorded at –269.4 °C (θ = 50°). (b), (c) Simulated spectra (dotted line: oriented component; broken line: nonoriented component).

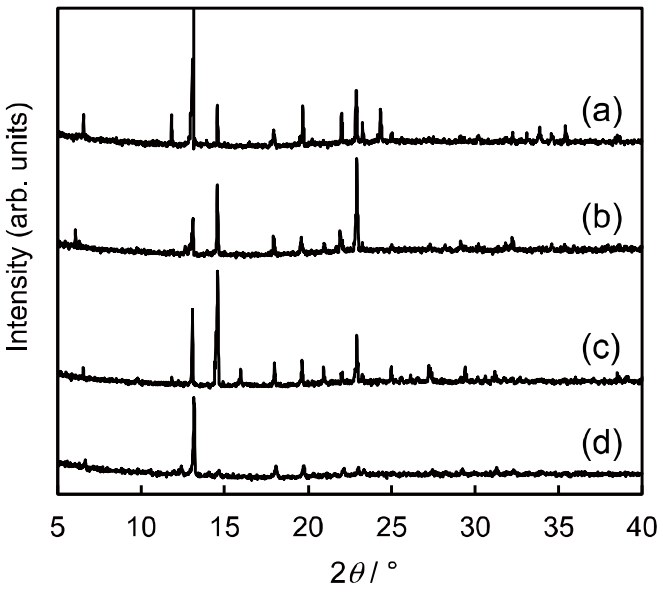

Fig. S6 Powder XRD patterns of [**C4Fc**][Tf_2N] crystallized under a magnetic field of 0.36 T (a–c) and without a magnetic field (d).

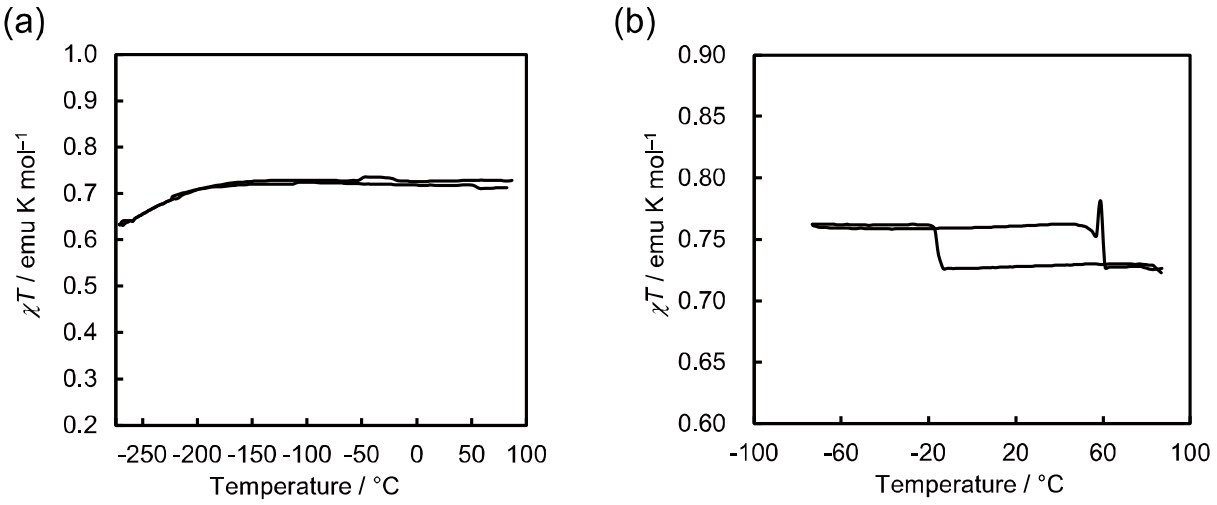

Fig. S7 Temperature dependences of magnetic susceptibilities of [**C5'Fc**][Tf_2N] measured under (a) 0.1 T and (b) 2 T at a scan rate of 2 °C min^{-1}.